Electrical Engineering (2024) 106:4821–4834
https://doi.org/10.1007/s00202-024-02271-5

ORIGINAL PAPER

Design and numerical analysis of thermal capability of power transformer using coupled electromagnetic field-thermal model

Yucel Cetinceviz[1] · Erdal Sehirli[2]

Received: 11 January 2024 / Accepted: 22 January 2024 / Published online: 11 February 2024

Abstract

In this study, by using the co-simulation technique, the dry-type transformer is designed for a wind turbine with 3.8 MVA, 690 V/36 kV power, and voltages. Dry-type transformers used in wind turbines require extra effort at the design stage concerning oil-immersed type because of the limited cooling capacity of air, possible higher inrush currents, resonant overvoltage, higher voltage, and load fluctuations that degrade thermal behavior. Furthermore, transformer design and analysis of their thermal behavior cannot be realized through one simulation software. Therefore, another approach using different simulation software simultaneously is needed, called co-simulation or multi-physics solution. This paper investigates transformer design and its effect on the system using a co-simulation technique including ANSYS Maxwell 3D, Simplorer, and Mechanical. After realizing the three-dimensional transformer design, its lumped parameter consisting of inductance matrix, leakage inductances, and resistances are determined analytically and using an eddy current solver. Core losses of the transformer, high- and low-voltage windings voltages, and their harmonic spectrums under different load conditions, including ohmic and inductive loads, are defined, the steady-state thermal solution is performed, and conclusions are made. It is proved that the transformer design works as desired.

Keywords Co-simulation · Inductance matrix · Inrush current · Multi-physics thermal analysis · Transformer design

1 Introduction

Due to the adverse effects of carbon-based energy sources on nature, the usage of renewable energy has gained much attention over the last few decades. One of the most important renewable energy sources is wind power. Wind power can be transformed into electrical energy using a wind turbine, generator, transformer, and gearbox. After obtaining electrical energy from a wind generator, to transfer this energy, a power transformer with high efficiency and minimal energy losses [1] should be used at the level of the distribution system [2] because it is not possible to store wind energy. So, this transformer used in wind energy generally has a step-up characteristic. Besides, the transformer can be a dry type or oil-cooled type [3, 4]. Concerning the oil-cooled transformer, dry-type of the transformer has the advantages of being non-flammability and lighter. So, it provides higher safety for the distribution of electrical systems. In addition, the more lightweight feature of dry type transformer makes the transformer located in the windmill nacelle possible [5, 6]. Also, the design procedure is different than designing a traditional distribution transformer; hence, the transformer's primary voltage changes with wind speed that has random characteristics. Also, the voltages may have harmonic content because of the arbitrary characteristic. So, a transformer for a wind turbine should overcome these two main problems: lower harmonic content and reliable power supply concerning changes in the wind speed and variable output conditions.

In addition, wind energy is transformed from wind power into electrical energy for the grid through some components that are wind turbine, gearbox, generator, power converter, and transformer.

In the literature, the design issue of transformers has found lots of interest; in [7], a review is made on wind turbine transformers. [8] designs a wind turbine using a 3D wound core. Protection methods of wind turbine transformers against

✉ Yucel Cetinceviz
ycetinceviz@kastamonu.edu.tr

Erdal Sehirli
erdal.sehirli@silicon-austria.com

1 Electrical and Electronics Engineering Department, Kastamonu University, Kastamonu, Turkey

2 Silicon Austria Labs GmbH, Graz, Austria

Table 1 Wind turbine transformers in the literature

Power	Low/high voltage (kV)	Reference
800 kVA	0.69/20	[8]
1.6 MVA	0.4/33	[25]
3.14 MVA	0.4/35	[26]
2.7 MVA	0.69/33	[27]
6.7 MVA	0.66/33	[28]
800 kVA	0.69/20	[10]
1.5 MVA	0.69/33	[29]
4 MVA	0.69/34	[30]

high-frequency transients are investigated [5, 9, 10], and analyses of wind turbine transformers on resonant overvoltage effects. An improved design considering the resonance problem because of the high-frequency transient for wind turbine transformers is realized in [11]. [12] compares the wind turbine and distribution transformers concerning dissolved gas that occurred due to the transformer's operation. Probabilistic analysis of switching transients of wind turbine transformers because of the breaker process is included in [13]. In [14], failure analysis of wind turbine transformers regarding over temperature is made. A 3-phase transformer model is established in the MATLAB Simulink environment to introduce a time domain model of a 3-phase, 2-winding transformer with nonlinear and hysteretic behavior [2]. Detailed three-phase transformer and inductance design are presented in [15]. In [16], power transformer windings deformation analysis in short circuit fault is analyzed by using the finite element method (FEM); also, in [17–19], by using FEM, power transformer transient analysis is realized. The power transformer is also modeled using FEM as in [20, 21]. Transformer design for wind turbines considering internal resonance is carried out in [22]. In [23], a three-phase rotary transformer is designed and analyzed for wind power application. The co-simulation technique is used and proved to be a convenient application for autotransformers [24]. Also, studies at different power and voltage ranges are given in Table 1.

It is still a common problem to design a transformer and provide its operation simultaneously in one simulation, even for distribution systems. The design and operation of the wind turbine transformer need extra care because of the randomly changing nature of the wind speed, resulting in different transformer voltages and variable outputs, as well as overvoltages due to the high-frequency transients. Besides, thermal analysis is crucial and must be considered in the correct design of electrical machines. Values of specific magnetic loading, electric loading, and current density for a particular electrical device should be limited to prevent overheating.

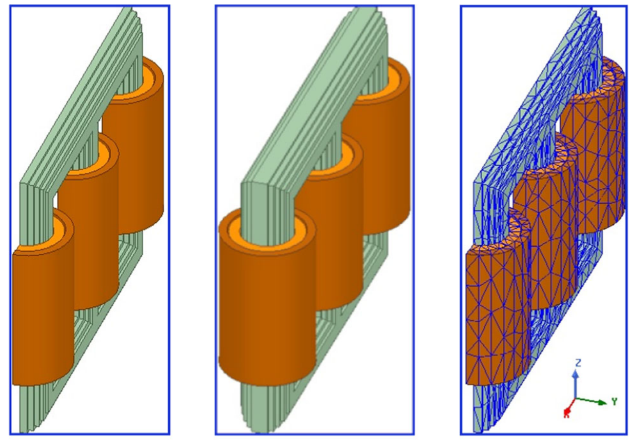

a) b) c)

Fig. 1 3-D model of the designed wind turbine transformer, **a** 3D symmetry model, **b** 3D full model, **c** mesh operation

In this paper, the phase dry type, step-up wind turbine transformer design is realized, and the effect of the designed transformer on the system is investigated using co-simulation techniques, including ANSYS Maxwell and Simplorer software. Furthermore, the core losses of the transformer, high- and low-voltage windings, and harmonic spectrums are presented. Also, the operation of the transformer under different load conditions, including ohmic and inductive loads, is analyzed. One of this study's most remarkable contributions is the multi-physics simulation consisting of a three-dimensional coupled electromagnetic field-circuit (co-simulation) and thermal analysis approach used to justify the analytical and three-dimensional FEM power transformer model. Unlike previously reported studies, the most significant contribution of this study is that it offers a practical model that includes no-load, full-load, short-circuit, in-rush current analysis and inductance matrix, leakage inductance, resistances calculation, and thermal analysis.

2 Three phase transformer design procedure for wind turbine

Before designing the transformer, it is good to visualize the structure of the transformer. Figure 1 shows a 3D model of the three-phase transformer and its windings, including a symmetric model, complete model, and mesh operation. This 3D model is realized by using ANSYS Maxwell 3D software. Applying symmetry boundary conditions to reduce computation time is always a good idea since the model needs to be refined for accurate analysis. This symmetry definition is equivalent to the complete model by applying the correct symmetry boundary condition, as shown in Fig. 1. Then, all parameters will be rescaled to account for the full

Table 2 Electrical and material properties of the design

Parameter		Values
Power		3.8 MVA
Voltage		0.69/36 kV
Frequency		50 Hz
Core material M270-35A (M19)	Mass density	7650 kg/m^3
	Frequency	50 Hz
	Thickness	0.35 mm
	Conductivity	1,923,000 S/m
	Kh	134.001 W/m^3
	Kc	0.387493 W/m^3
	Ke	1.17493 W/m^3
Winding material		Copper
Phase number		3

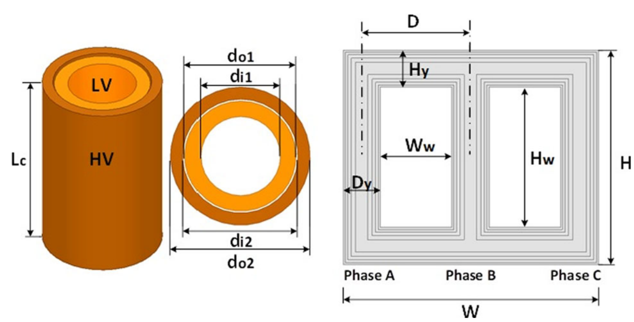

Fig. 2 Transformer core, windings, and dimension descriptions

model by setting symmetry multiplier 2 (symmetry factor). Besides, starting with a suitable mesh operation is essential to reduce computation time and provide accurate analysis [24]. A length-based mesh is created throughout the volume of the core and windings. Also, the maximum number of elements is set to 10,000 for core and windings.

While designing the transformer, main electrical parameters such as power, voltage, and frequency should be defined, and the material of the transformer core type of conductor should be chosen. In Table 2, the parameters that are required to design the transformer are given.

In Fig. 1, a 3D model of the transformer is given. Also, in Fig. 2, a 2D model of the transformer is shown; in that figure, the transformer core, phase windings, and dimension descriptions of the core are given as it is seen that three-phase windings of the transformer are wounded as shell-type. HV and LV are defined as high voltage and low voltage, respectively.

Transformer power can be written concerning induced winding voltage, (φ_{m}) maximum flux in (Wb), number of turns, and frequency as in (1). Also, induced voltage per turn E_{t} can be summarized in (2). In (2), r is a constant that is a ratio of φ_{m} to AT, shown in (3). Also, AT means ampere turn given in (3). Besides, f is frequency, N_2 is the number of turns of high voltage windings, ph is a phase, and I_s is phase current in (1)–(3) as in [15]. Also, K is a constant that typically changes between 0.6 and 0.7 for three-phase transformers.

$$\begin{aligned} S &= 3 \times U_{\mathrm{HV}} \times I_S \cong E_{\mathrm{HV}} \times I_S \\ &= 3 \times 4.44 \times f \times \varphi_{\mathrm{m}} \times N_2 \times I_s \end{aligned} \tag{1}$$

$$E_{\mathrm{t}} = \frac{U_{\mathrm{HV}}}{N_2} = \sqrt{4.44 \times f \times r} \times \left(\sqrt{\frac{S}{\mathrm{ph}}}\right) = K \times \sqrt{\frac{S}{\mathrm{ph}}} \tag{2}$$

$$r = \frac{\varphi_{\mathrm{m}}}{\mathrm{AT}}; \quad \mathrm{AT} = N_2 \times I_s \tag{3}$$

In a transformer, the dimension of the transformer is proportional to the transformer power level. In (4), the cross-sectional area (A_i) equation of the core is given, and it consists of induced voltage, frequency, and maximum flux density (B_{m}) in Tesla. In (4), the (d) core diameter equation is given, and k_{c} refers to the stepped core coefficient. The width of the yoke (D_{Y}) is shown in (5), and k_i is the stacking factor. Also, the height of the yoke (H_{Y}) can be calculated using (5). In (6), the window area (A_{W}) equation is given, K_{W} is the window space factor, and J is the current density. In (7) and (8), window width (W), frame width (W), and frame height (H) can be calculated. Besides, the ratio of ($H_{\mathrm{W}}/W_{\mathrm{W}}$) changes between 2 and 4 in three-phase power transformers.

$$A_i = \frac{E_{\mathrm{t}}}{4.44 \times f \times B_{\mathrm{m}}}; \quad d = \sqrt{\frac{A_i}{k_{\mathrm{c}}}} \tag{4}$$

$$H_E = \frac{A_i}{D_{\mathrm{Y}}}; \quad D_{\mathrm{Y}} = k_i \times d \tag{5}$$

$$A_{\mathrm{W}} = \frac{E_{\mathrm{t}}}{3.33 \times f \times B_{\mathrm{m}} \times K_{\mathrm{W}} \times J \times 10^6 \times A_i} \tag{6}$$

$$W = 2W_{\mathrm{W}} + 3D_{\mathrm{Y}}; \quad W_{\mathrm{W}} = \frac{A_{\mathrm{W}}}{H_{\mathrm{W}}} \tag{7}$$

$$H = H_{\mathrm{w}} + 2H_{\mathrm{y}} \tag{8}$$

One of the most essential characteristics of designing a magnetic material is the *B–H* curve, which defines the saturation of the transformer. The *B–H* curve of the M270-35A material is given in Fig. 3a. It is seen that close to 2 T, the core has saturation. Therefore, 1.5 T is chosen as the maximum flux density in the design.

The other important characteristic of the core is the between core loss and flux density, as shown in Fig. 3b for the M270-35A core. It is seen by the figure that core loss changes with magnetic flux density, so while designing a transformer,

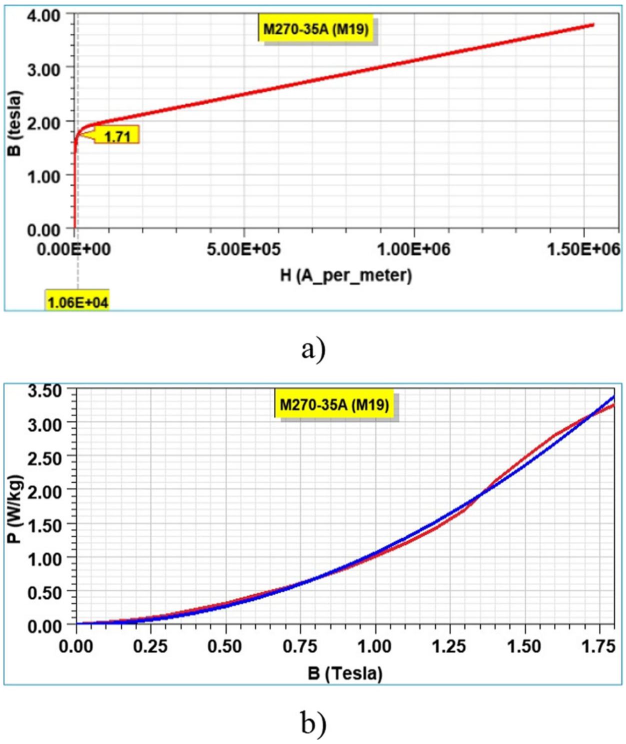

Fig. 3 Magnetic properties of the M270-35A material, **a** *B*–*H* curve; **b** core loss-magnetic flux density curve

Table 3 Calculated dimension of the transformer

Required dimensions	
Width of yoke (D_{Y})	270 mm
Height of yoke (H_{Y})	255 mm
Distance between the core center (D)	750 mm
Width of window (W_{W})	480 mm
Height of window (H_{W})	961 mm
Width of frame (W)	1770 mm
Height of frame	1486 mm
Cross-sectional area (A_{i})	0.057 m^2

a convenient flux density should be chosen to reduce core loss and not to provide saturation. Also, in Fig. 3b, constant parameters, K_h, K_c, and K_e, used in the design calculation are given.

Using (1)–(8), calculated dimensions' values of the transformer for the desired are calculated and given in Table 3 with the description as in Fig. 2.

In the design of windings for three-phase transformers, the connection type of the windings is essential. In this study, LV windings are connected, and the nominal voltage is 690 V. On the other hand, HV windings are connected as Y, and the nominal voltage is chosen as 36 kV.

Table 4 Calculated parameters

Design parameters	LV	HV
Number of turns	40	1260
Turns ratio	0,03	
Cross-sectional area of conductor	615mm^2	23.32mm^2
Conductor diameter winding	28 mm	5.5 mm
The outer diameter of the winding	394 mm	494 mm
The mean length of winding	1.06 m	1.41 m
Winding resistance	0.705mΩ	1.14Ω
Winding connection	Delta (Δ)	Star (Y)

For LV windings, (9) and (10) are used to calculate the conductor's number of turns and diameter. N_1, I_p, a_p, j, and d_p refer to LV winding number of turns, LV winding phase current rms value, a cross section of conductor, current density, and conductor diameter, respectively.

$$N_1 = \frac{U_{\mathrm{LV\_ph}}}{E_{\mathrm{t}}} \tag{9}$$

$$d_p = 2 \times \sqrt{\frac{a_p}{\pi}}; \quad a_p = \frac{I_p}{J}; \quad I_p = \frac{S}{3 * U_{\mathrm{LV\_ph}}} \tag{10}$$

For HV windings, (11) and (12) are used to calculate the number of turns and the diameter of the conductor. Also, N_2, I_{s}, a_{s}, J, d_{s} refer to the HV winding number of turns, HV winding phase current rms value, a cross section of conductor, current density, and conductor diameter, respectively.

$$N_2 = N_1 \times \frac{U_{\mathrm{HV\_ph}}}{U_{\mathrm{LV\_ph}}} \tag{11}$$

$$d_s = 2 \times \sqrt{\frac{a_s}{\pi}}; \quad a_s = \frac{I_s}{J}; \quad I_s = \frac{S}{3 * U_{\mathrm{HV\_ph}}} \tag{12}$$

After the design of three three-phase transformers, calculated parameters regarding HV and LV windings are given in Table 4.

2.1 Inductance calculation for designed transformer

Precise inductance value calculation is critical in transformer design [31]. Figure 4a and b shows three phase three, limb core type, and magnetic circuit of three-phase transformers, respectively. The magnetic field in the transformer is analyzed by applying the excitation current. Symmetrical excitation currents are used for the magneto-motive forces ($\boldsymbol{F_{LV\_a}= N_{LV}\ i_a}$, $\boldsymbol{F_{LV\_b}= N_{LV}\ i_b}$ and $\boldsymbol{F_{LV\_c}= N_{LV}\ i_c}$) required to produce instantaneous values of fluxes ($\boldsymbol{\Phi_a}$, $\boldsymbol{\Phi_b}$ and $\boldsymbol{\Phi_c}$). The reluctance of a core section or air region as a limb of the magnetic circuit is obtained by magnetic energy

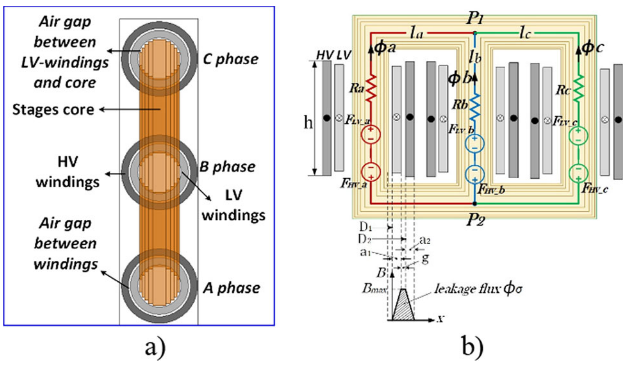

Fig. 4 The three-phase transformer studied **a** the structure of the two winding and limb core types and **b** the equivalent magnetic circuit of the transformer for inductance calculations and length of the magnetic path of phases [33, 34]

and magnetic flux related to magnetic areas of the core [32]. It is clear from Fig. 4b that there is a natural asymmetry in the core as the length of the magnetic path of phase B between the points P1 and P2 is less than that of phases A and C.

Using the superposition theorem to equivalent magnetic circuit [35] of the transformer at no load, instantaneous values of fluxes ($\boldsymbol{\Phi_a}$, $\boldsymbol{\Phi_b}$, and $\boldsymbol{\Phi_c}$) in every limb can be figured out by Eqs. (13)–(15), respectively [34].

$$\Phi_a = \frac{N_{\mathrm{LV}} \times i_a(t)}{R_a + \frac{R_b \times R_c}{R_b + R_c}} - \frac{R_c}{R_a + R_c} \cdot \frac{N_{\mathrm{LV}} \times i_b(t)}{R_b + \frac{R_a \times R_c}{R_a + R_c}} - \frac{R_b}{R_a + R_b} \cdot \frac{N_{\mathrm{LV}} \times i_c(t)}{R_b + \frac{R_a \times R_b}{R_a + R_b}} \quad (13)$$

$$\Phi_b = -\frac{R_c}{R_b + R_c} \cdot \frac{N_{\mathrm{LV}} \times i_a(t)}{R_a + \frac{R_b \times R_c}{R_b + R_c}} + \frac{N_{\mathrm{LV}} \times i_b(t)}{R_b + \frac{R_a \times R_c}{R_a + R_c}} - \frac{R_b}{R_a + R_b} \cdot \frac{N_{\mathrm{LV}} \times i_c(t)}{R_c + \frac{R_a \times R_b}{R_a + R_b}} \quad (14)$$

$$\Phi_c = -\frac{R_b}{R_b + R_c} \cdot \frac{N_{\mathrm{LV}} \times i_a(t)}{R_a + \frac{R_b \times R_c}{R_b + R_c}} - \frac{R_a}{R_a + R_c} \cdot \frac{N_{\mathrm{LV}} \times i_b(t)}{R_b + \frac{R_a \times R_c}{R_a + R_c}} + \frac{N_{\mathrm{LV}} \times i_c(t)}{R_c + \frac{R_a \times R_b}{R_a + R_b}} \quad (15)$$

The reluctance R_b represents the leg of the core, R_a, and R_c represent the sum of the yoke and leg of the core. In this asymmetric configuration, the reluctance of the A-phase and C-phase is considered exact ($R_a = R_c = R$), and magnetic path lengths are $\ell_a = \ell_c = l$. Also, it is assumed that cross-sectional areas are $A_a = A_b = A_c = A$, and all phases have the same turns $N_{\mathrm{LV\_}a} = N_{\mathrm{LV\_}b} = N_{\mathrm{LV\_}c} = N_{\mathrm{LV}}$. Besides, reluctance can be computed as follows;

$$R_a = R_c = \frac{l}{\mu \times A}, \qquad R_c = \frac{l_b}{\mu \times A} \quad (16)$$

Here, $\mu = B/H$ is magnetic permeability [H/m]. Since the flux linkages are $\lambda_1 = N_{\mathrm{LV}}\ \phi_a$, $\lambda_2 = N_{\mathrm{LV}}\ \phi_b$, $\lambda_3 = N_{\mathrm{LV}}\ \phi_c$ and this transformer configuration, as shown in Fig. 4b, marks that phase winding one is coupled to all windings (1–6), the following matrix form can be written;

$$\begin{bmatrix} \lambda_1(t) \\ \vdots \\ \lambda_6(t) \end{bmatrix} = \begin{pmatrix} L_{11} & \dots & L_{16} \\ \vdots & \ddots & \vdots \\ L_{61} & \cdots & L_{66} \end{pmatrix} \times \begin{bmatrix} i_1(t) \\ \vdots \\ i_6(t) \end{bmatrix} \quad (17)$$

The self and mutual inductance terms (L_{ii} and L_{ij}) of the **L** matrix are obtained from excitation currents at a nominal frequency, while LV three-phase winding is excited and the other HV three-phase winding is open. Subscripts 1–3 and 4–6 indicate LV and HV winding, respectively. Self-inductances (L_{ii}) [36] of three phase transformer can be found in the first term of Eqs. (13)–(15) and mutual inductances (L_{ij}) can be seen from the other six terms of Eqs. (13)–(15) as follows;

$$L_{11} = \frac{N_{\mathrm{LV}}^2}{R_a + \frac{R_b \times R_c}{R_b + R_c}}, \quad L_{22} = \frac{N_{\mathrm{LV}}^2}{R_b + \frac{R_a \times R_c}{R_a + R_c}}, \quad L_{66} = \frac{N_{\mathrm{HV}}^2}{R_c + \frac{R_a \times R_b}{R_a + R_b}},$$
$$L_{12} = \frac{R_c}{R_a + R_c} \cdot \frac{N_{\mathrm{LVa}} \times N_{\mathrm{LVb}}}{R_b + \frac{R_a \times R_c}{R_a + R_c}}, \quad L_{16} = \frac{R_b}{R_b + R_c} \cdot \frac{N_{\mathrm{LVa}} \times N_{\mathrm{HVc}}}{R_a + \frac{R_b \times R_c}{R_b + R_c}},$$
$$L_{21} = \frac{R_c}{R_b + R_c} \cdot \frac{N_{\mathrm{LVa}} \times N_{\mathrm{LVb}}}{R_a + \frac{R_b \times R_c}{R_b + R_c}}, \quad L_{26} = \frac{R_a}{R_a + R_c} \cdot \frac{N_{\mathrm{LVb}} \times N_{\mathrm{HVc}}}{R_b + \frac{R_a \times R_c}{R_a + R_c}} \quad (18)$$

Also, the mutual inductance of windings can be calculated by the coupling coefficient between each phase and windings [20]. Magnetization and leakage inductance calculation using magnetic energy (W) stored in the windings and the gap is the most accurate. Using Ampere's law, the magnetization inductance (L_{m}) can be expressed as follows [37];

$$N_{\mathrm{LV}} \times I_{\mathrm{m}} = \frac{B_{\mathrm{core}}}{\mu_0 \times \mu_r} l_\phi \quad (19)$$

$$B_{\mathrm{core}} = \frac{\mu_0 \times \mu_r}{l_\phi} \times N_{\mathrm{LV}} \times I_{\mathrm{m}} \quad (20)$$

$$W = \frac{1}{2} L_{\mathrm{m}} \times I_{\mathrm{m}}^2 = \frac{1}{2} \int_v \vec{H} \times \vec{B} \times \mathrm{d}v \quad (21)$$

$$\frac{L_{\mathrm{m}} I_{\mathrm{m}}^2}{2} = \frac{1}{2} \frac{B_{\mathrm{core}}^2}{\mu_0 \mu_r} V = \frac{1}{2\mu_0 \mu_r} \left(\frac{\mu_0 \times \mu_r}{l_\phi} N_{\mathrm{LV}} I_{\mathrm{m}} \right)^2 l_\phi A \quad (22)$$

$$L_{\mathrm{m}} = \frac{N_{\mathrm{LV}}^2 \times \mu_0 \times \mu_r \times A}{l_\phi} \quad (23)$$

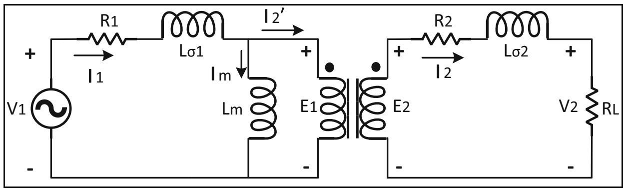

Fig. 5 Lumped model of transformer [36]

where I_m is magnetization current and can be calculated by $I_{LV} - I_{HV}/(turn\ ratio)$, B_{core} is the magnetic flux density of the core, and ℓ_ϕ is the magnetic path length of the core. Then, leakage or short circuit inductance (L_σ) can be derived in a similar approach to magnetization inductance applying a flux diagram as shown in Fig. 5b as follows;

$$L_\sigma = \frac{N_{LV}^2 \cdot \mu_0 \cdot A}{h} \cdot \pi \cdot \left(\frac{a_1 \cdot D_1 \cdot a_2 \cdot D_2}{3} + g \cdot D_g \right) \quad (24)$$

where h is the height of windings, a_1, a_2, and ag are the radial lengths, and D_1, D_2, and D_g are the mean diameters of LV, HV, and gap, respectively.

2.2 Eddy current analysis to extract lumped parameters for designed transformer

Figure 5 shows a phase-lumped model of the transformer. FEM is the most widely used numerical method for lumped parameter calculation [18] of structure and asymmetric flux distributions that cannot be accurately evaluated by an analytical approach [20]. The main advantage of the 3D FEM is that any complex geometry can be solved because the formulas run on finite elements depend solely on the problem class and are independent of its geometry. In this study, the eddy current solver calculates time-varying magnetic fields in a frequency domain and is used to obtain lumped parameters in a steady state. Energy, torques, forces, and inductances can be calculated from fundamental field quantities such as magnetic and scalar potential. The results obtained from this solution and analytical results are given comparatively in Table 5. For instance, self-inductance L_{11} (LV_a, LV_a) was calculated as follows,

$$L_{11} = \frac{N_{LV}^2}{R_a + \frac{R_b \times R_c}{R_b + R_c}} = \frac{N_{LV}^2}{\frac{1}{\mu A} \times \left(l + \frac{l_b \cdot l}{l_b + l} \right)}$$
$$= \frac{40^2}{\frac{1}{2.11 \times 10^{-3} \times 0.057} \times \left(2.716 + \frac{1.216 \times 2.716}{1.216 + 2.716} \right)}$$
$$= 54.22 \text{ mH}$$

It is clear from Table 5 that there is symmetry between phases A and B. Also, a natural asymmetry of phase B. Result shows that the analytical method agrees with the FEM.

Table 5 Lumped parameters of designed transformer

Parameters	FEM	Analytical
L_{11} (LV_a, LV_a)	54.394 mH	54.22 mH
L_{22} (LV_b, LV_b)	72.871 mH	72.623 mH
L_{33} (LV_c, LV_c)	54.389 mH	54.22 mH
L_{44} (HV_a, HV_a)	53.924 H	53.799 H
L_{55} (HV_b, HV_b)	72.289 H	72.102 H
L_{66} (HV_c, HV_c)	53.929 H	53.799 H
L_{12} (LV_a, LV_b)	35.842 mH	35.674 mH
L_{13} (LV_a, LV_c)	17.243 mH	17.113 mH
L_{14} (LV_a, HV_a)	1.71 H	1.706 H
L_{15} (LV_a, HV_b)	1.13 H	1.124 H
L_{16} (LV_a, HV_c)	0.543 H	0.528 H
L_{23} (LV_b, LV_c)	35.844 mH	35.657 mH
L_{24} (LV_b, HV_a)	1.129 H	1.12 H
L_{25} (LV_b, HV_b)	2.293 H	2.287 H
L_{26} (LV_b, HV_c)	1.13 H	1.12 H
L_σ (LV_a)	0.12 mH	0.13 mH
L_σ (LV_b)	0.091 mH	0.097 mH
L_σ (HV_a)	0.049 H	0.05 H
L_σ (HV_b)	0.0457 H	0.0478 H
L_m (LV_a)	54.275 mH	54.148 mH
L_m (LV_b)	72.779 mH	72.589 mH
Resistance $R_1 = R_2 = R_3$	0.697 mΩ	0.72 mΩ
Resistance $R_4 = R_5 = R_6$	1.15 Ω	1.22 mΩ

3 Co-simulation study of the designed transformer

The design and validation of electrical machines require complex processes. This is expected to be an expensive and time-consuming process. Accordingly, any simulation and analysis model must be up to this case. This section utilizes the co-simulation study using ANSYS Maxwell and ANSYS Simplorer software. Direct and indirect coupling are two basic co-simulation approaches to couple electromagnetic fields with circuits. This study uses the direct coupling approach, where a circuit model can transiently solve the Maxwell 3D FE model [38]. It offers an excellent solution to have extensive data related to transformer behavior in different operational conditions.

The 3D FE model of the transformer, designed in Sect. 2, is placed in the circuit simulation model to analyze its operation characteristics under different load conditions, as shown in Fig. 6. It is seen that the transformer is connected as Δ-Y connection. Also, $R1$, $R2$, R3, $R4$, $R5$, $R6$ are the winding resistance and $R7$, $R8$, $R9$ are load. In Table 6, simulation parameters and scenarios are given.

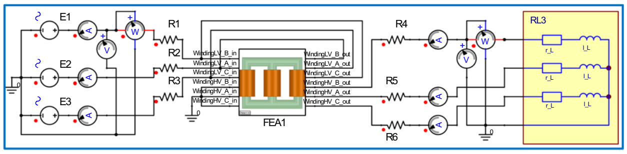

Fig. 6 Simulation circuit consisting of co-simulation

Table 6 Simulation parameters

Simulation parameters		
Power	3.8 MVA	
Voltage	690/36 kV	
Frequency	50 Hz	
Scenario	Load-1	No load
	Load-2 (*R*)	354 Ω
	Load-3 (RL)	283 Ω–0.68 H
	Load-4 (variable)	250–400–600–100 Ω

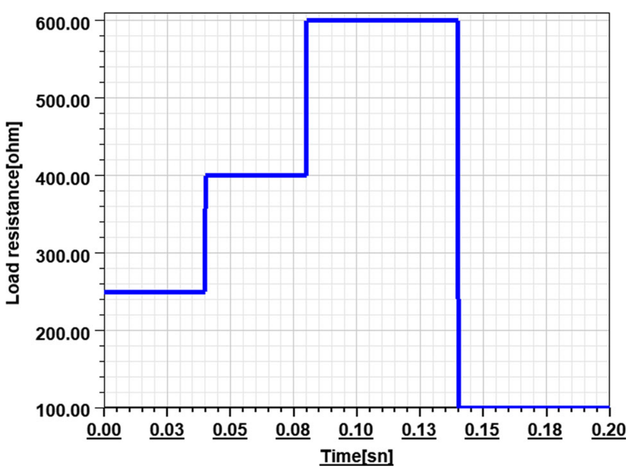

Fig. 7 Variable load used in simulation

A voltmeter, ammeter, wattmeter, and load bank are connected at the output terminals of delta-connected HV windings. Input terminals of LV windings are supplied with a 3-phase, 563.3 V (Vpeak), 50 Hz voltage source that is star-connected. At first, the 3-phase input voltage waveforms are obtained by variation of phase shifting taps, and an exponentially increasing voltage source has been applied to eliminate high inrush currents and a long simulation time as follows [39];

- $E1 = V_{\text{peak}} * (1 - \exp(-50t)) * \cos(2 * \text{pi} * 50t)$
- $E2 = V_{\text{peak}} * (1 - \exp(-50t)) * \cos(2 * \text{pi} * 50t + (2/3 * \text{pi}))$
- $E3 = V_{\text{peak}} * (1 - \exp(-50t)) * \cos(2 * \text{pi} * 50t + (4/3 * \text{pi}))$

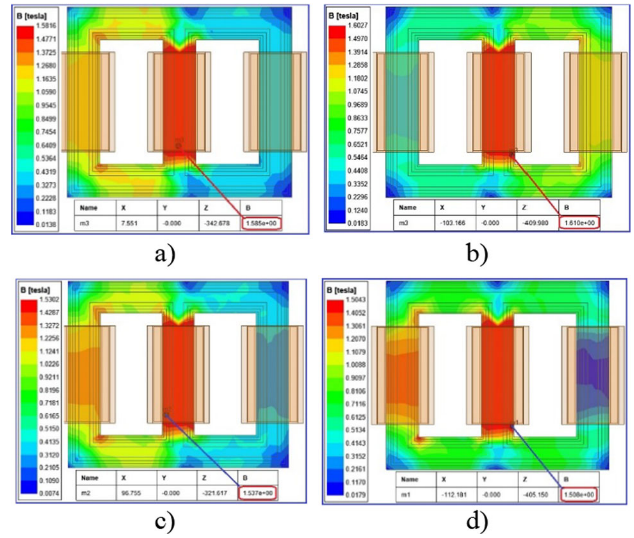

Fig. 8 Magnetic flux density of core at **a** no load; **b** full ohmic load; **c** RL load; **d** variable load

Figure 7 shows the variable load used in the simulation study and its change time. At the beginning load is 250 Ω, then it is changed to 400 Ω at 0.04 s and 600 Ω at 0.08 s then to 100 Ω at 0.142 s.

3.1 Flux density

The core flux density can be expressed as follows [18, 40]:

$$B = \frac{1}{N_s \times A_e} \int_0^t v(\tau) \times d\tau \tag{25}$$

where v is the secondary winding voltage, N_s is the number of sense winding turns, and A_e is the effective cross section of the core.

The magnetic field is mainly affected by ferromagnetic material with high relative permeability [40]. So, M270-35A (M19) has high permeability is chosen. In Fig. 8, the magnetic flux density of the core is given at full load is 354 Ω by finite element analysis (FEA).

The flux density distributions in the whole section of the core (Fig. 8) are obtained at 178 ms. It is seen in Fig. 8 that the magnetic flux density of the body is under the saturation limit (1.7 T) convenient to the design in Sect. 2. The center leg of the transformer is close to the maximum of 1.61 T magnetic flux density for rated voltage with full ohmic 354Ω load, as shown in Fig. 8b. Thereby, the hysteresis losses of the transformer are forecasted to be very low.

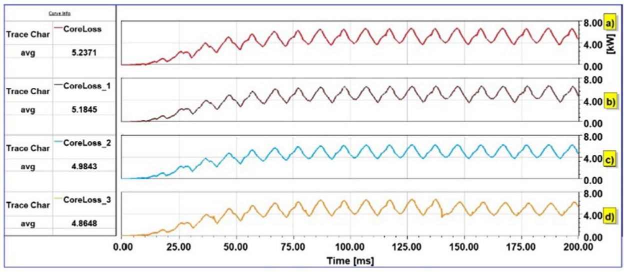

Fig. 9 Core losses of M270-35A (M19) core, **a** no load; **b** full ohmic load; **c** RL load; **d** variable load

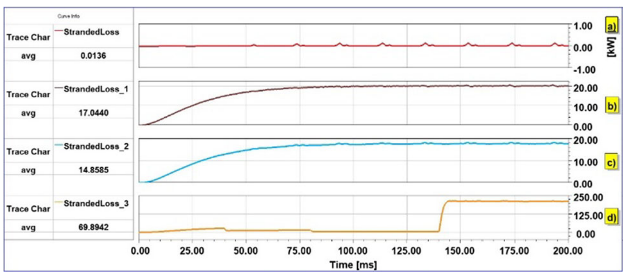

Fig. 10 Stranded loss of transformer, **a** no load; **b** full ohmic load; **c** RL load; **d** variable load

3.2 Losses of designed transformer

Specifying losses in a transformer is a critical assignment that must be fulfilled during the electromagnetic analysis [41]. Using the 3D FEM model for the electromagnetic analysis of transformers provides to obtain numerical values of losses [42, 43]. The determination of accurate data for the *B–P* curve of the electrical steel material has a distinct effect on the accuracy of this analysis. So, the accurate data provided by the materials manufacturers are entered, as shown in Fig. 3.

The total loss of the transformer mainly comprises copper loss (winding) and core loss. The core loss involves hysteresis, eddy current, and additional losses [1, 41, 44]. The core loss is expressed in the frequency domain [42, 43] under sinusoidal flux conditions as follows:

$$P = K_{\mathrm{h}} B_{\max}^{2} f + K_{c} (B_{\max} f)^{2} + K_{e} (B_{\max} f)^{1.5} \qquad (26)$$

where K_{h}, K_c, and K_e are the hysteresis, eddy, and additional loss coefficient, respectively, $B_{\max}$ is the maximum amplitude of the flux density, and f is the frequency. The copper loss or stranded loss is a resistive loss in a 2D or 3D volume in windings which has multi-turn coils and stranded type are determined as follows:

$$P_{\mathrm{st}} = \frac{1}{\sigma} \times \int_{V} J^{2} \times \mathrm{d}V \qquad (27)$$

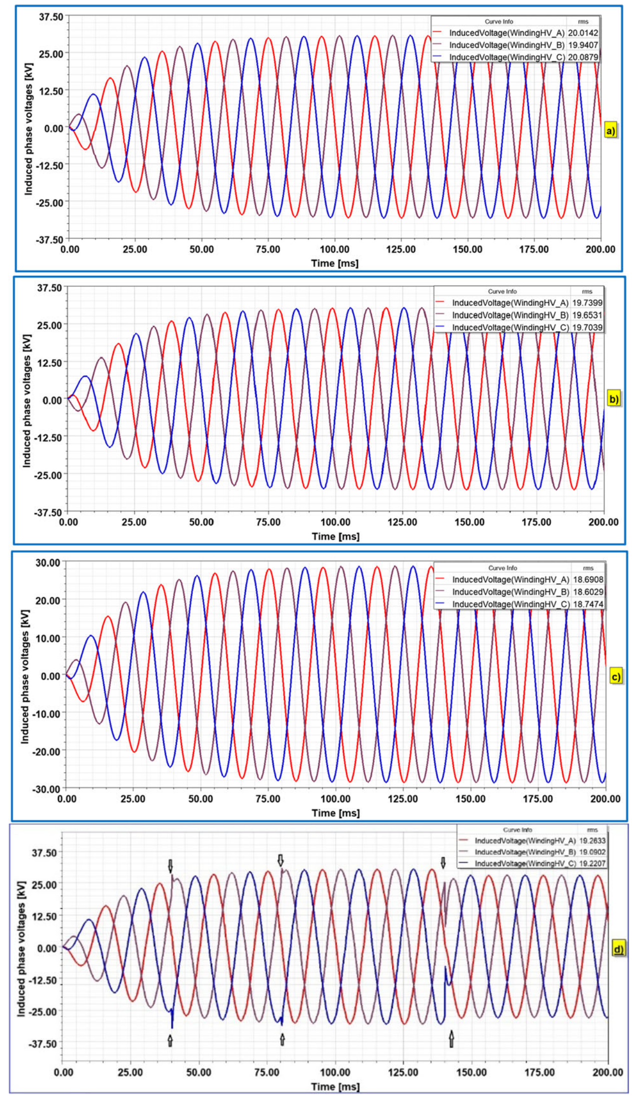

Fig. 11 HV windings induced voltages, **a** no load; **b** full ohmic load; **c** RL load; **d** variable load

where σ is electrical conductivity, J is current density, and V is winding volume. Core losses consisting of hysteresis and eddy losses of the transformer are also crucial for the efficiency of the transformer. In Fig. 9, core losses are given concerning the different load conditions.

The average core losses are 5.23 kW, 5.18 kW, and 4.98 kW at no, complete, and RL loads, respectively. At variable load in Fig. 9d, core loss is also around 4.86 kW. Core loss is called a no-load loss of an electrical machine. Although considered constant, it may vary slightly depending on voltage and frequency for different operational conditions, as shown in Fig. 9 [1]. It is clear from Fig. 9 that core loss decreases in voltage decreases for various load conditions.

The transient solution for the stranded loss of the transformer is given in Fig. 10. These quick solutions are carried out within 0.002 s steps between 0 and 0.2 s for achieving

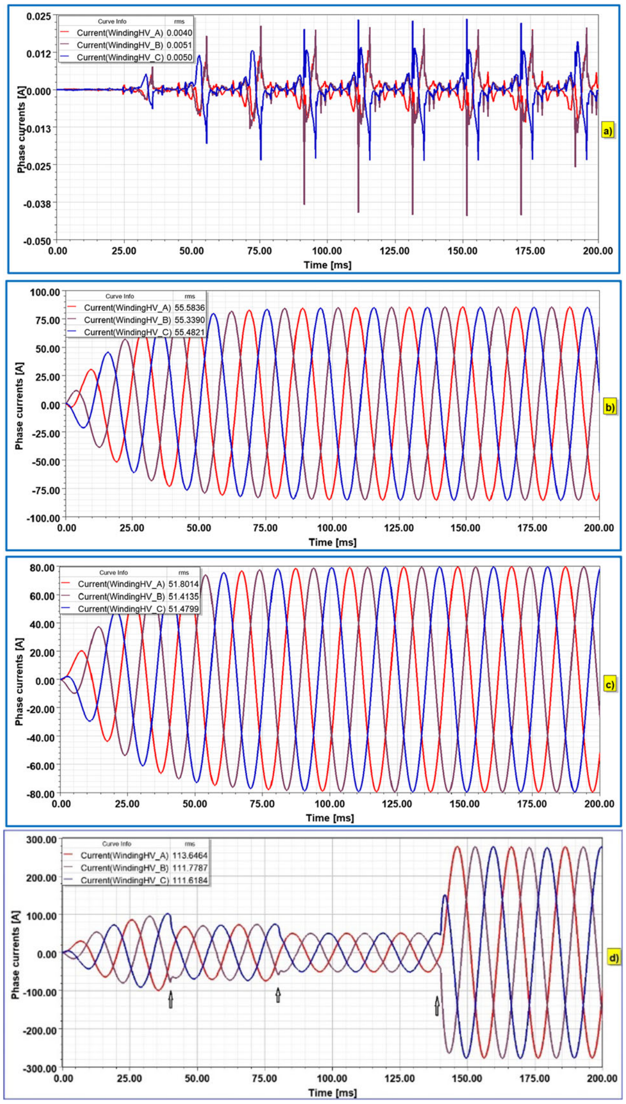

Fig. 12 HV windings phase currents, **a** no load; **b** full ohmic load; **c** RL load; **d** variable load

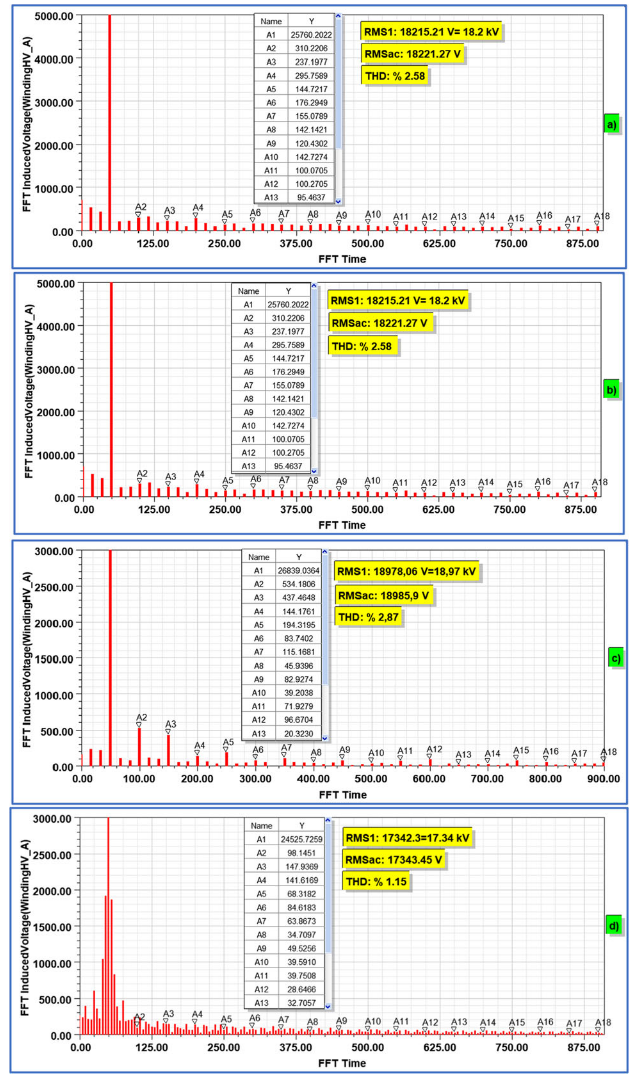

Fig. 13 HV windings induced voltages harmonic spectrum, **a** no load; **b** full ohmic load; **c** RL load; **d** variable load

accuracy in results. It can be observed that the stranded loss has reached a steady state at 100 ms. It is seen that stranded losses are 17 kW and 14.85 kW for full load and RL load, respectively. At variable load in Fig. 10d, the stranded loss is also around 69.89 kW. It is especially seen that the stranded loss increases where the load value is unexpectedly increased at 142 ms.

3.3 Performance of designed transformer

To observe HV and LV windings voltages, and their harmonic spectrums, under different load conditions, including ohmic and inductive loads, a 3D FEM coupled circuit model is established, as shown in Fig. 6 [24]. In Fig. 11, phase voltages of secondary windings of the transformer, that is, HV windings, namely induced voltages, are given by different load conditions.

It is seen in Fig. 11a–d that induced voltages are sinusoidal with minor unbalanced conditions, some notches, and voltage drops because of overloading, respectively. Besides, HV windings phase currents are given in Fig. 12 with different load conditions, full load, full RL load, and variable load. It is possible to assert that the transformer is giving a proper reaction, significantly where the load value is abruptly increased. Some fluctuations have been observed because of sudden changes in load.

On the other hand, harmonic spectrum analysis for each induced phase voltage, as shown in Fig. 13, and the total harmonic distortion (THD) is 2.58%, 2.87%, and 1.15% for each phase, respectively. When the FFT chart of induced HV voltage is investigated, it is clear that the inductive load

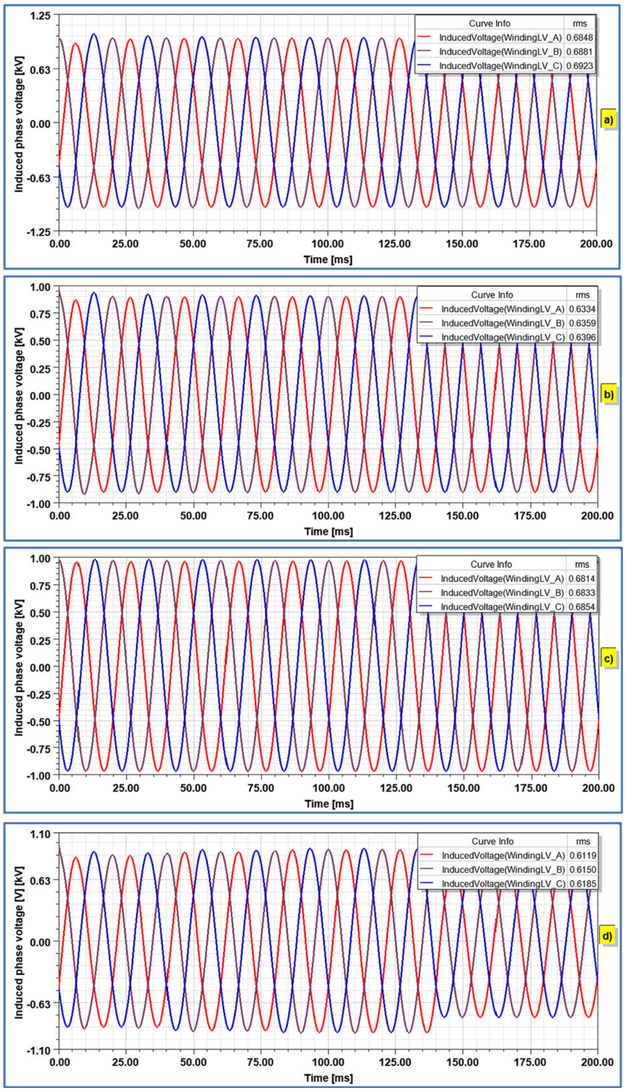

Fig. 14 LV windings phase voltages, **a** no load; **b** full ohmic load; **c** RL load; **d** variable load

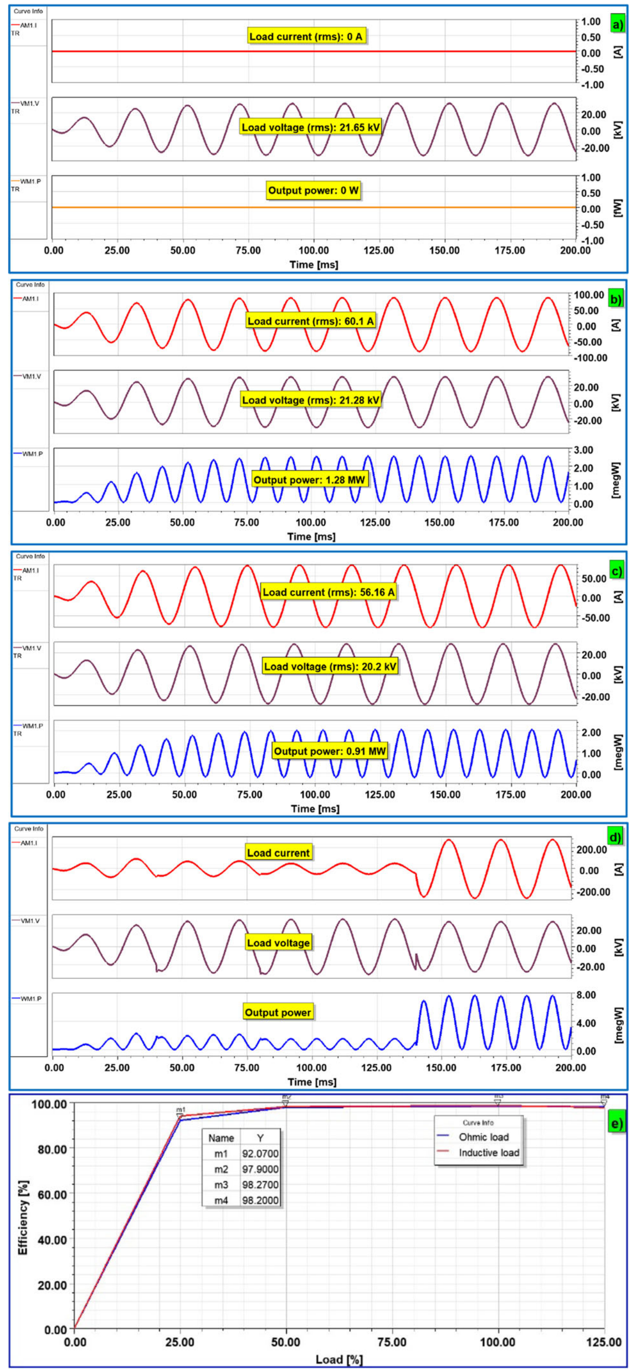

Fig. 15 Transformer performance, **a** no load; **b** full ohmic load; **c** RL load; **d** variable load; **e** efficiency curves

increases the distortion of the sine wave compared to the ohmic load (Fig. 13b and c).

LV windings phase voltages are also given in Fig. 14 under different load conditions.

In Fig. 15, transformer performance characteristics are given under different load conditions: no load, full load, full RL load, and variable load. Figure 15e shows the efficiency curve of varying load conditions (no load, 25% load, 50% load, 100% load, and 125% loads), including ohmic and inductive loads. The efficiency curve shows that the efficiency of the transformer increases by 92–98.27% up to the rate. The efficiency of the transformer at variable load is 96.59% on average. So, the voltage, current, power, and efficiency trends show good agreement as a transformer performance. So, it is easily applicable for an on-grid operating system of wind turbines.

Primary windings (LV windings) are set at rated conditions and fed through the rated voltage in a coupled external circuit to conduct inrush analysis. Then, secondary windings (HV windings) are open-circuited. In the second step, the exponentially increasing voltage source is removed to see the effects of the inrush current as follows;

Table 7 Performance of designed transformer

Parameters	Value			
	No load	R load (rated)	R-L load (rated)	Variable load (avg)
Output power	–	3.84 MW	2.73 MW	4.98 MW
HV Induced voltage (ph)	21.81 kV	21.48 kV	20.35 kV	19.26 kV
LV Induced voltage (ph)	693.33 V	689.2 V	690.46 V	680 V
Load current	–	60.1 A	56.16 A	195.49 A
Terminal voltage (ph to ph)	37.49 kV	36.85 kV	34.98 kV	33.84 kV
Frequency	50 Hz	50 Hz	50 Hz	50 Hz
Efficiency	–	98.27%	98.6%	96.6%
Voltage regulation	–	1.12%	5%	–

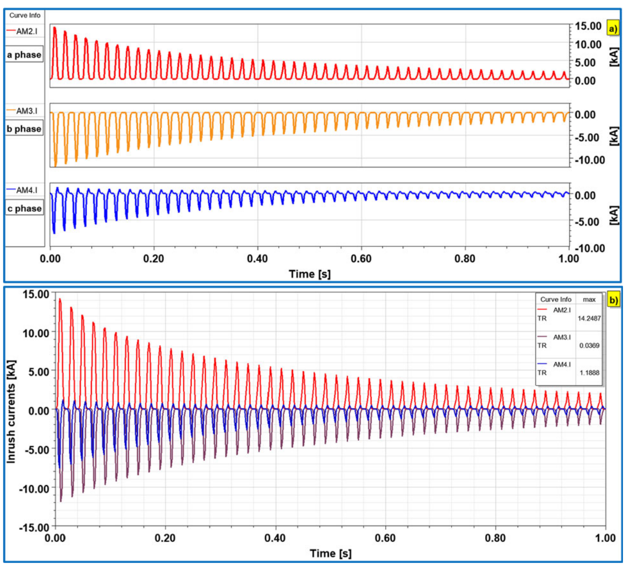

Fig. 16 Inrush currents, **a** phase currents, **b** three-phase currents

- $E1 = V_{peak} * \cos(2 * \text{pi} * 50t)$
- $E2 = V_{peak} * \cos(2 * \text{pi} * 50t + (2/3 * \text{pi}))$
- $E3 = V_{peak} * \cos(2 * \text{pi} * 50t + (4/3 * \text{pi}))$

Consequently, quantities of interest are inrush transient transformer current for a time duration of 1 s, as shown in Fig. 16. The peak value of the inrush current culminates nine times the transformer at a nominal load current. The current becomes a steady-state condition after 0.6 s. Power capacitors used in power systems cause this transient to increase. Current differential relays are used to protect transformers from the effects of this inrush.

In addition, all of the performance values are summarized in Table 7. It shows that the designed transformer meets the grid demand. It provides pure sinusoidal voltage and current where the grid conditions change. Especially at overload, the efficiency of a transformer is about 98.2%.

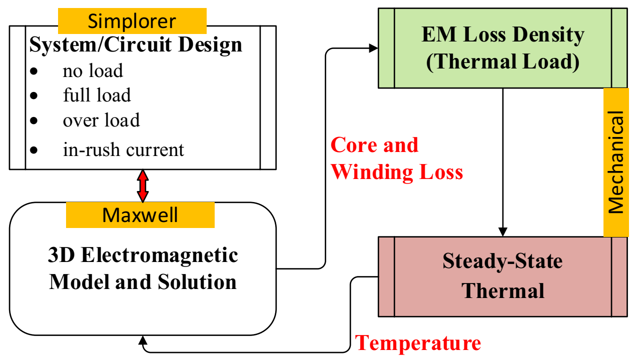

Fig. 17 Multi-physics solution model

3.4 Coupled electromagnetic field-thermal analysis

In Fig. 17, a multi-physics solution model of coupled electromagnetic and thermal analysis is given. In this model, the temperature dependence of the material properties on both the thermal and electromagnetic sides should be considered, and the materials' electrical and mechanical properties should be defined. The first 3D electromagnetic model determines core and winding losses; losses are directly coupled into the thermal simulation as the thermal load to obtain temperature distribution. Lastly, the resulting temperature is coupled as feedback into the electromagnetic side to change the permeability and conductivity of the material.

Losses are given in Table 8 and imported into the thermal simulation as the thermal load to obtain temperature distribution. A scaling factor enclosed to 1 means proper network and loss mapping from magnetic field solution to steady-state thermal setup.

Figure 18 shows the temperature distribution of the entire body of the transformer for different operations. As expected, the maximum temperature is 43 °C in the core 31 °C in the LV and HV winding at no load operation, as shown in Fig. 18a. The temperature of the core limbs, which are in direct contact with the windings, is higher than that of the core back. As

Table 8 Imported loss density with scaling at full load operation

Object	Total loss	Scaling factor
Core	4496.23 W	1.00048
HV_C	2250.9 W	0.984874
LV_C	1374.15 W	0.97623
HV_A	2240.38 W	0.989194
HV_B	2243.97 W	0.983994
LV_A	1383.16 W	0.982679
LV_B	1371.61 W	0.989328

expected, the maximum temperature is 108 °C in the LV winding and 106 °C in the HV winding during the entire load operation, as shown in Fig. 18b. The average temperature on the whole body is 93.23 °C. In addition, the maximum temperature is 105 °C at 25% overload (RL) and 125 degrees at 25% overload (*R*), as shown in Fig. 18d and e.

Fan cooling systems can be employed with natural convection to decrease temperature. Natural convection is a cheap and suitable way for heat transfer. It is commonly used in dry-type power transformers.

4 Conclusion

In this paper, 3.8 MVA power, 690 V/36 kV three-phase transformer design for wind turbine is realized. After designing the transformer, its lumped parameters analytically and by using an eddy current solver. Thanks to the electromagnetic field, circuit, and thermal model, including three different software, Ansys Maxwell, Simplorer, and Mechanical, used in this paper, transformer core losses, harmonic spectrums under various load conditions, and thermal distribution of all bodies are measured. Transient solutions in co-simulation are carried out within 0.2 ms steps between 0 and 200 ms to obtain more accurate results.

This paper shows that the transformer designed has low core loss values with different load conditions, that is, 5.23 kW, 5.18 kW, 4.98 kW, and 4.86 kW. Besides, under various load conditions, the harmonic spectrum of the secondary (HV) windings voltage is measured as 2.58%, 2.87%, and 1.15%, lower than the values stated in standard IEC, and resulting phase currents are obtained sinusoidal. The efficiency, voltage regulation, and average temperature of the proposed transformer are about 99%, 1.12%, and 93.23 °C, respectively, at full load. So it is pretty good and acceptable. Furthermore, it is also shown that the co-simulation technique presented in this paper for wind turbine transformers works appropriately.

It is essential to realize that a finite element model cannot consider all physical core loss effects, such as mechanical stress on laminations and edge burr losses. Hence, as a future work, a FEM multi-physics simulation structure will be used to couple 3D FEM electromagnetic, steady-state thermal, and structural analyses. This enables the import of core and stranded losses computed in the electromagnetic field into the thermal analysis module and then the structural analysis module to determine steady-state temperatures and deformations.

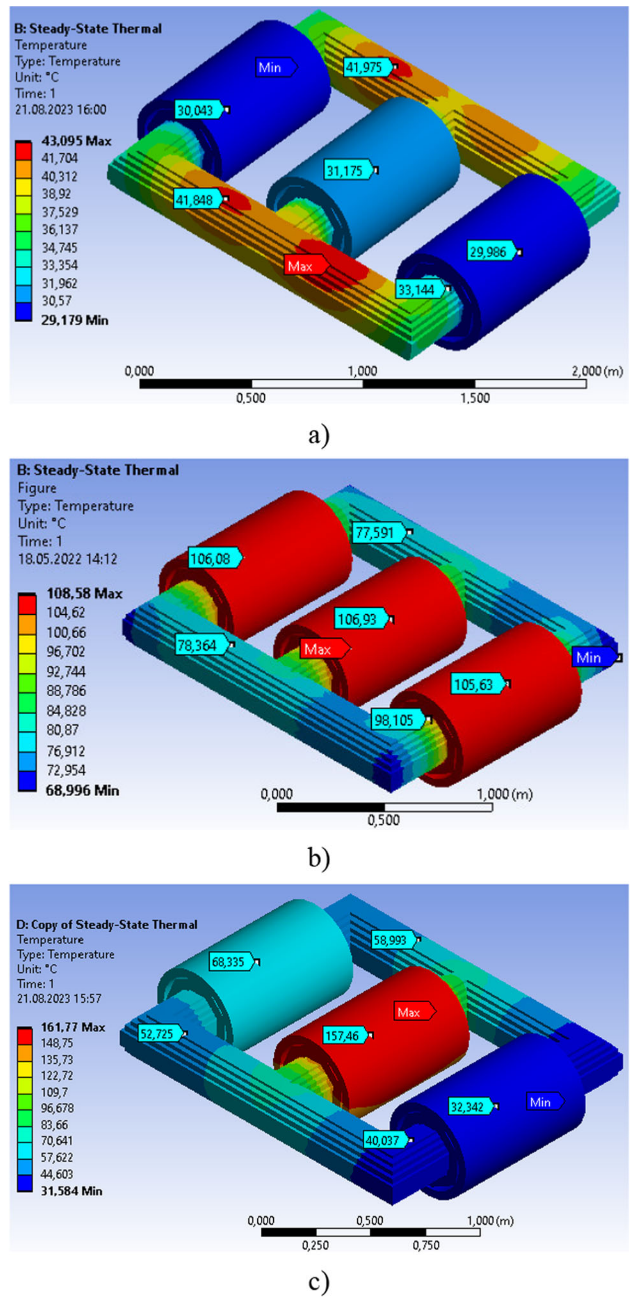

Fig. 18 Temperature distribution of transformer for different operations: **a** no load, **b** full load, **c** in-rush current at transient regime, **d** at 25% overload (RL), **e** at 25% overload (*R*)

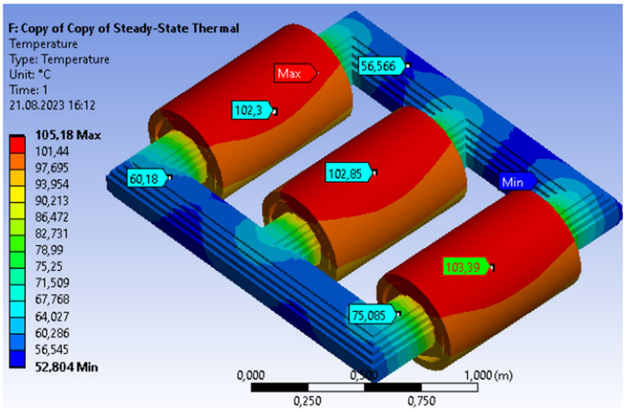

d)

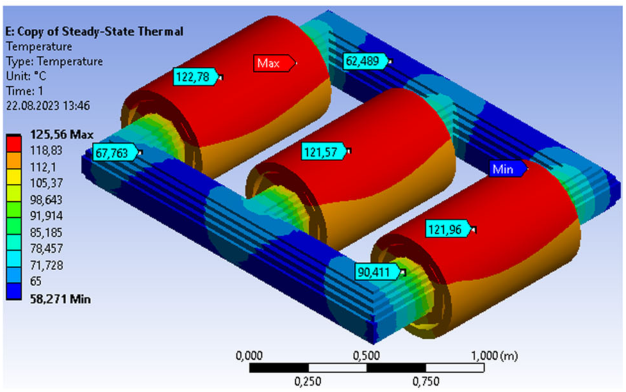

e)

Fig. 18 continued

Author contributions YC conceived the analysis. YC and ES performed the analysis and collected data. YC and ES wrote the main manuscript text, and YC prepared all figures. All authors reviewed the manuscript

Data availability No data were used for the research described in the article.

Declarations

Conflict of interest The authors report that there are no competing interests to declare.

References

1. Isık F, Uyaroglı Y (2015) Amorphous core transformers efficiency analysis in Turkish electrical distribution systems. Turk J Electr Eng Comput Sci 23(6):1523–1535
2. Ozgonenel O, Guney KRI, Usta O, Dirik H (2012) A novel three-phase transformer hysteresis model in MATLABTM Simulink. Turk J Electr Eng Comput Sci 20(4):479–492
3. Özgönenel O, Thomas D (2017) Modeling and simulation of 2.5 MVA SF6-gas-insulated transformer. Turk J Electr Eng Comput Sci 25(4):3475–3485
4. Özgönenel O, Thomas D, Kurt Ü (2018) SF6 gas-insulated 50-kVA distribution transformer design. Turk J Electr Eng Comput Sci 26(4):2140–2150
5. Smugala D, Piasecki W, Ostrogorska M, Florkowski M, Fulczyk M, Granhaug O (2015) Wind turbine transformers protection method against high-frequency transients. IEEE Trans Power Delivery 30(2):853–860
6. Meier S, Kjellqvist T, Norrga S, Nee HP (2009) Design considerations for medium-frequency power transformers in offshore wind farms. In: 13th European conference on power electronics and applications IEEE, pp 1–12
7. Jose G, Chacko R (2014) A review on wind turbine transformers. In: 2014 Annual international conference on emerging research areas: magnetics, machines and drives (AICERA/iCMMD). IEEE, pp 1–7
8. Elhaminia P, Moradnouri A, Vakilian M (2015) Wind turbine transformer optimum design assuming a 3D wound core. In: 30th International power system conference (PSC). IEEE, pp 38–44
9. Soloot AH, Høidalen HK, Gustavsen B (2015) Influence of the winding design of wind turbine transformers for resonant overvoltage vulnerability. IEEE Trans Dielectr Electr Insul 22(2):1250–1257
10. Soloot AH, Høidalen HK, Gustavsen B (2015) Modeling wind turbine transformers to analyze resonant overvoltages. Electr Power Syst Res 115:26–34
11. Elhaminia P, Vakilian M, Lehtonen M (2018) Wind turbine transformer improved design method entailing resonance blocking. IET Electr Power Appl 12(9):1337–1343
12. Singh P, Blackburn T (2018) Dissolved gas analysis results in wind turbine transformers. In: 2018 Australasian Universities power engineering conference (AUPEC). IEEE, pp 1–6
13. Ghasemi S, Allahbakhshi M, Behdani B, Tajdinian M, Popov M (2020) Probabilistic analysis of switching transients due to vacuum circuit breaker operation on wind turbine step-up transformers. Electr Power Syst Res 182:106204
14. Zhu YM, Gong Y, Yang ZG (2019) Failure analysis on overtemperature combustion of transformers in 4 MW offshore wind turbines. Eng Fail Anal 96:211–222
15. McLyman CWT (2004) Transformer and inductor design handbook. CRC Press, Boca Raton
16. Zhang H, Yang B, Xu W, Wang S, Wang G, Huangfu Y, Zhang J (2013) Dynamic deformation analysis of power transformer windings in short-circuit fault by FEM. IEEE Trans Appl Supercond 24(3):1–4
17. Ostrenko M, Andriienko B (2017) Transformer impulse surges calculation by FEM coupled to the circuit. IEEE Trans Magn 53(6):1–4
18. Khaligh A, Vakilian M (2008) Power transformers internal insulation design improvements using electric field analysis through finite-element methods. IEEE Trans Magn 44(2):273–278
19. Marketos F, Marnay D, Ngnegueu T (2012) Experimental and numerical investigation of flux density distribution in the individual packets of a 100 kVA transformer core. IEEE Trans Magn 48(4):1677–1680
20. Wang R, Xiao F, Zhao Z, Shen Y, Yang G (2014) Effects of asymmetric coupling on winding AC resistance in the medium-frequency high-power transformer. IEEE Trans Magn 50(11):1–4
21. Jimenez-Mondragon VM, Escarela-Perez R, Melgoza E, Arjona MA, Olivares-Galvan JC (2017) Quasi-3-D finite-element modeling of a power transformer. IEEE Trans Magn 53(6):1–4
22. Elhaminia P, Vakilian M (2016) Frequency response features of a multi-objective wind turbine transformer design. In: 2016 24th Iranian conference on electrical engineering (ICEE). IEEE, pp 643–648
23. Zhong H, Zhao L, Wang X, Li X (2015) Design and analysis of a three-phase rotary transformer for doubly fed induction generators.

In: 2014 IEEE industry application society annual meeting. IEEE, pp 1–6
24. Ugale RT, Mejari KD, Chaudhari BN (2018) Intermediate voltage variation-based interconnecting transformer design for voltage and phase angle control with coupled field FEA studies. IEEE Trans Ind Electron 65(8):6077–6088
25. Arana I, Hernandez A, Thumm G, Holboell J (2011) Energization of wind turbine transformers with an auxiliary generator in a large offshore wind farm during islanded operation. IEEE Trans Power Deliv 26(4):2792–2800
26. Badrzadeh B, Gustavsen B (2012) High-frequency modeling and simulation of wind turbine transformer with doubly fed asynchronous generator. IEEE Trans Power Deliv 27(2):746–756
27. Banda CA, Van Coller JM (2015) Resonant overvoltages in wind turbine transformers. In: 2015 IEEE Eindhoven PowerTech. IEEE, pp 1–6
28. Thiede A, Kaltenborn U, Hensel M (2019) Field diagnosis on transformers for wind turbine applications. In: 2019 IEEE PES GTD grand international conference and exposition Asia (GTD Asia). IEEE, pp 554–558
29. Ma T, Cadmore A (2005) System studies of voltage dips resulting from energization of MV wind turbine transformers. In: 18th International conference on electricity distribution, Turin.
30. Kersiulis V, Holdyk A, Holboell J, Arana I (2012) Sensitivity of nodal admittances in an offshore wind power plant to parametric variations in the collection grid. In Proceedings of the 11th international workshop on large-scale integration of wind power into power systems.
31. Dawood K, Cinar MA, Alboyaci B, Sonmez O (2019) Calculating the leakage reactance in distribution transformers via numerical and analytical methods. J Electr Syst 15(2):213–221
32. Wang Y, Yuan J (2018) Calculation approach of reluctance in the magnetic circuit of transformer employed to convert into an equivalent electric circuit. COMPEL Int J Comput Math Electr Electron Eng 37(5):1668–1677
33. Zhu L, Yoon HS, Cho HJ, Um DJ, Koh CS (2015) Finite-element analysis of magnetostriction force in power transformer based on the measurement of anisotropic magnetostriction of highly grain-oriented electrical steel sheet. IEEE Trans Magn 52(3):1–4
34. Matsumori H, Shimizu T, Takano K, Ishii H (2018) Three-phase AC filter inductor design for three-phase PWM inverter for conversion efficiency improvement at low load. Electr Eng Jpn 203(1):37–49
35. Saraiva E, Chaves ML, Camacho JR (2008) Three-phase transformer representation using FEMM, and a methodology for air gap calculation. In: 2008 18th International conference on electrical machines. IEEE, pp 1–6
36. Prochazka R, Hlavacek J, Draxler K (2015) Magnetic circuit of a high-voltage transformer up to 10 kHz. IEEE Trans Magn 51(1):1–4
37. Hameyer K (2001) Electrical machines 1: basics, design, function, operation. Institut für Elektrische Maschinen an der RWTH Aachen
38. Cetinceviz Y, Sehirli E, Uygun D, Ocak C, Demirel H (2019) Transient analysis with coupled field-circuit model and experimental assessment of a PMSG used in a small-scale wind turbine for water heating purposes. Electr Eng 101:1163–1175
39. Al-Dori O, Şakar B, Dönük A (2022) Comprehensive analysis of losses and leakage reactance of distribution transformers. Arab J Sci Eng 47(11):14163–14171
40. Strac L, Kelemen F, Zarko D (2009) Modeling and calculation of electromagnetic field in the surroundings of a large power transformer. Turk J Electr Eng Comput Sci 17(3):301–314
41. Muhlethaler J, Biela J, Kolar JW, Ecklebe A (2011) Improved core-loss calculation for magnetic components employed in power electronic systems. IEEE Trans Power Electron 27(2):964–973
42. Bahmani MA, Agheb E, Thiringer T, Høidalen HK, Serdyuk Y (2012) Core loss behavior in high frequency high power transformers—I: effect of core topology. J Renew Sustain Energy 4(3)
43. Agheb E, Bahmani MA, Høidalen HK, Thiringer T (2012) Core loss behavior in high frequency high power transformers—II: arbitrary excitation. J Renew Sustain Energy 4(3)
44. Tikhonova O, Malygin I, Beraya R, Sokolov N, Plastun A (2017) Loss calculation of induction motor with ring windings by ANSYS Maxwell. In: Actual problems of electromechanics and electrical technologies APEET-2017. Yekaterinburg, pp 63–66